Modelling of induction machines with skewed rotor slots

A.Tenhunen and A.Arkkio

Abstract: A model permitting the simulation of induction machines with skewed rotor slot is presented. The two-dimensional finite-element method is used for electromagnetic field analysis of the induction machine. The skew effects are considered by coupling several discs cut by planes perpendicular to the shaft. The solution of the resulting nonlinear time-dependent equation is obtained using step-by-step numerical integration. The paper also presents a method to avoid the singular matrices when rotor bar currents are solved from field and circuit equations. The model is verified by comparing measured and computed results for a 37kW cage induction motor. Current and voltage waveforms and torque–speed curves are discussed. According to the results the model gives good results when the slip value is under 0.9.

1 Introduction

Skewed rotor slots were originally used to provide starting torque when the motors had equal numbers of stator and rotor slots [1]. This technique was kept later even though knowing that starting torque could be provided by choosing a proper number of rotor slots. It was proved that other negative influences such as asynchronous torque harmonics, oscillating torque and stray load losses could be reduced when skewed rotor slots were used.

Progressive improvement in the power and speed of workstations has resulted in a situation in which time-stepping finite-element analysis of electrical machines is used as an industrial tool. For most types of electrical machines, the modelling is two-dimensional. Their potentially more accurate three-dimensional counterparts require one or two orders of magnitude more of computer resources, so they are still well beyond the bounds of economic viability [2].

The rotor skew in induction machines is a problem for two-dimensional calculation because of the axial variations in the magnetic field due to the changing orientation of rotor with respect to stator [3]. In an analytical method, skewing can be modelled using a skew-factor [4]. In a numerical method, the skewing is quite often modelled using so called multislice technique. It is possible to use separate field and circuit models when the induced rotor bar currents are time-stepped but the field equations are not [2]. If the field and electric equations are in the same matrix, they are solved simultaneously. Usually in this case, the variables are vector potential, the potential differences over the slice in rotor slots and stator currents [5, 6]. Dziwniel and Piriou [7] used a hybrid 3D approach using the 2D invariant hypothesis to model skew. In their model the end ring currents and scalar potential were solved instead of rotor bar currents or potential differences. We propose a multislice time-stepped model in which field and electric equations are solved in the same matrix and the solved variables are magnetic vector potential, rotor bar and stator currents. The rotor bar currents are normally not used as a variable in calculation. In some cases (when periodicity factor is equal to one), a straight use of rotor bar currents as variables is not possible because of singular matrices. This paper also presents a method to avoid the singular matrices when rotor bar currents are solved from field and circuit equations.

IEE Proceedings online no. 20010036

DOI: 10.1049/ip-epa:20010036

Paper first received 22nd May and in revised form 13th September 2000

The authors are with Helsinki University of Technology, Laboratory of Electromechanics, P.O. Box 3000, 02015 HUT, Finland

2 Numerical model

The modelling of an induction machine can be done using two-dimensional electromagnetic field equations in which the geometry and magnetic material characteristics are independent of z co-ordinate. In this kind of a model, the rotor slot skewing and other three-dimensional effects have to be taken into account within the two-dimensional model [8]. An approach to represent a skewed rotor in two dimensions is to use a set of two-dimensional models. The magnetic fields of the slices are coupled together by forcing the currents of rotor bars and stator winding to be continuous from slice to slice. The angle difference between each slice is modelled by

$$\alpha = \alpha_0 + \gamma \frac{2n - n_{tot} - 1}{2n_{tot}} \tag{1}$$

in which α and α_0 are angles between rotor and stator with and without skew, γ is skew angle, n is number of slice and n_{tot} is total number of slices. From Maxwell's equations and by introducing the magnetic vector potential $\boldsymbol{A}$ and electric scalar potential ϕ, we obtain the partial differential equation

$$\nabla \times (\nu \nabla \times \boldsymbol{A}) + \sigma \frac{\partial \boldsymbol{A}}{\partial t} + \sigma \nabla \phi = 0 \tag{2}$$

in which ν is the magnetic reluctivity and σ is the electric conductivity. When the two-dimensional model is used to calculate a straight conductor of length $l^{(m)}$ of one slice, the scalar potential difference U between the ends of the

conductor in the slice is given by

$$U = -\int_{\Gamma} \nabla\phi dl = -\nabla\phi_1 l^{(m)} \tag{3}$$

If R is used the DC resistance of the conductor, the voltage equation of the slice becomes

$$U = RI + R\int_S \sigma\frac{\partial \boldsymbol{A}}{\partial t}dS \tag{4}$$

in which I is total current and S is the area of the cross-section of the conductor. If the total current is taken as a source of the field, the vector potential satisfies the integro-differential equation [9]

$$\nabla\times(\nu\nabla\times\boldsymbol{A})+\sigma\frac{\partial \boldsymbol{A}}{\partial t}-\frac{\sigma R}{l^{(m)}}\int_S \sigma\frac{\partial \boldsymbol{A}}{\partial t}\cdot dS\,\boldsymbol{e}_z = \frac{\sigma R}{l^{(m)}}I\boldsymbol{e}_z \tag{5}$$

If the thickness of the slices is always the same i.e. $l^{(1)} = l^{(2)} = \ldots = l^{(m)} = l/m$, eqn. 5 can be written

$$\nabla\times(\nu\nabla\times\boldsymbol{A}) + \sigma\frac{\partial \boldsymbol{A}}{\partial t} - \frac{1}{S}\int_S \sigma\frac{\partial \boldsymbol{A}}{\partial t}\cdot dS\,\boldsymbol{e}_z = \frac{1}{S}I\boldsymbol{e}_z \tag{6}$$

In the time-stepped finite-element method the field equations have to be solved by a step-by-step method evaluating the variation of the field in short time intervals Δt. In the Crank–Nicholson method, the vector potential at time step $k + 1$ is approximated

$$\boldsymbol{A}_{k+1} = \frac{1}{2}\left\{\left.\frac{\partial \boldsymbol{A}}{\partial t}\right|_{k+1} + \left.\frac{\partial \boldsymbol{A}}{\partial t}\right|_{k}\right\}\Delta t + \boldsymbol{A}_k \tag{7}$$

2.1 Equations for rotor cage

Normally in FEM calculations, stranded conductors have current excitation and solid conductors have voltage excitation. In this work, in rotor bars, current excitation is used in solid conductors instead of traditional potential difference excitation. In this way the continuity of currents from slice to slice is included directly into the matrix equations.

To shorten expressions, the circuit equations of the rotor are derived for sinusoidally varying quantities. The same solution method is applicable in the case of general time variation, but the equations are considerably longer. Only the results are given for the time-stepped case.

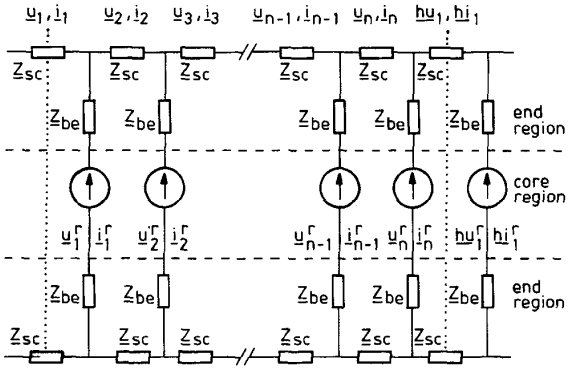

Fig. 1 *Circuit model of rotor cage in which h is periodicity factor*

Fig. 1 shows the circuit notations used in the derivation of the circuit equation for the rotor cage. Impedance matrices associated with the bar ends and end ring segments are defined [9]

$$\begin{aligned}\underline{\boldsymbol{Z}}_{be} &= 2\underline{\boldsymbol{Z}}_{be}\mathbf{1}\\ \underline{\boldsymbol{Z}}_{sc} &= 2\underline{\boldsymbol{Z}}_{sc}\mathbf{1}\end{aligned} \tag{8}$$

where $\mathbf{1}$ denotes the diagonal unit matrix. The total potential difference vector of the rotor bars including the bar ends outside the slice model is

$$\underline{\boldsymbol{u}}^{r'} = \underline{\boldsymbol{u}}^{r} + \underline{\boldsymbol{Z}}_{be}\underline{\boldsymbol{i}}^{r} \tag{9}$$

From Kirchhoff's second law applied to the circuit of Fig. 1, a relation between the potential difference vectors is obtained

$$2\underline{\boldsymbol{u}} = \begin{bmatrix} 1 & 0 & 0 & \cdot & -h \\ -1 & 1 & \cdot & \cdot & 0 \\ 0 & -1 & 1 & \cdot & \cdot \\ \cdot & \cdot & \cdot & \cdot & \cdot \\ 0 & 0 & \cdot & \cdot & 1 \end{bmatrix}\underline{\boldsymbol{u}}^{r'} = \boldsymbol{M}\underline{\boldsymbol{u}}^{r'} \tag{10}$$

where $\underline{\boldsymbol{u}}$ is the end ring potential difference and h is periodicity factor (±1). Kirchhoff's first law gives the connection between the end ring currents $\underline{\boldsymbol{i}}$ and the rotor bar currents $\underline{\boldsymbol{i}}^r$, respectively

$$\underline{\boldsymbol{i}}^{r} = \begin{bmatrix} -1 & 1 & 0 & \cdot & 0 \\ 0 & -1 & 1 & \cdot & 0 \\ 0 & 0 & -1 & \cdot & \cdot \\ \cdot & \cdot & \cdot & \cdot & 1 \\ h & 0 & 0 & \cdot & -1 \end{bmatrix}\underline{\boldsymbol{i}} = -\boldsymbol{M}^T\underline{\boldsymbol{i}} \tag{11}$$

The potential differences in the end ring segments between adjacent rotor bars are given by

$$2\underline{\boldsymbol{u}} = \underline{\boldsymbol{Z}}_{sc}\underline{\boldsymbol{i}} \tag{12}$$

Combining eqns. 8–12 obtains the relation between the rotor bar currents and the potential differences of the bars induced in the core region

$$(1 + \boldsymbol{M}^T\underline{\boldsymbol{Z}}_{sc}^{-1}\boldsymbol{M}\underline{\boldsymbol{Z}}_{be})\underline{\boldsymbol{i}}^{r} = -(\boldsymbol{M}^T\underline{\boldsymbol{Z}}_{sc}^{-1}\boldsymbol{M})\underline{\boldsymbol{u}}^{r} \tag{13}$$

Now the potential difference $\underline{\boldsymbol{u}}^r$ can be solved from eqn. 13. Unfortunately, the product of matrices on the right side of eqn. 13 is singular if the periodicity factor is equal to one. In this case we need an additional constraint that is obtained by studying the potential differences of the end rings and rotor bar currents. If the periodicity factor is equal to one, the sum of the end ring potential differences is zero and the sum of the bar currents is zero. Provided that

— all rotor bars have equal impedance

— the end ring segments all have equal impedance

— the periodicity factor is equal to one

the sum of the end ring currents is zero and the sum of end ring potential difference is zero. This means that the multiplication of the end ring current vector $\underline{\boldsymbol{i}}$ and potential difference vector of the rotor bar $\underline{\boldsymbol{u}}^r$ by matrix $\boldsymbol{K}_b$, whose elements are all equal to one, for example, gives the zero column vector, i.e. $\boldsymbol{K}_b \cdot \underline{\boldsymbol{i}} = 0$ and $\boldsymbol{K}_b \cdot \underline{\boldsymbol{u}}^r = 0$. These zero vectors are added to eqns. 10 and 11. As a result, a nonsingular coefficient matrix product is obtained and the voltage difference of rotor bars $\underline{\boldsymbol{u}}^r$ can be solved from eqn. 13.

The relationship between $\underline{\boldsymbol{u}}^r$ and $\underline{\boldsymbol{i}}^r$ can be changed from time-harmonic form to a time-stepped form using eqn. 7. Another relationship can be obtained from the electric eqn. 4. The rotor bar currents have to be continuous from slice to slice. Eqn. 4 can then be written for a rotor bar

$$\sum_1^m \boldsymbol{D}_m^r\boldsymbol{A}_{k+1} + \sum_1^m \boldsymbol{D}_m^r\boldsymbol{A}_k + \frac{\Delta t}{2l}\left[1 + \frac{1}{R_r}\left[\left((\boldsymbol{K}_b + \boldsymbol{M})^T(\boldsymbol{K}_b + \boldsymbol{M})\right)^{-1}\right.\right.$$

$$\cdot \left(\left(R_{sc} + 2\frac{L_{sc}}{\Delta t}\right) + \left(R_{be} + 2\frac{L_{be}}{\Delta t}\right) \cdot \left((\boldsymbol{K}_b + \boldsymbol{M})^T(\boldsymbol{K}_b + \boldsymbol{M})\right)\right]\Big] \boldsymbol{i}^r_{k+1} + \frac{\Delta t}{2l}\left[1 + \frac{1}{R_r}\left[\left((\boldsymbol{K}_b + \boldsymbol{M})^T(\boldsymbol{K}_b + \boldsymbol{M})\right)^{-1} \cdot \left(\left(R_{sc} - 2\frac{L_{sc}}{\Delta t}\right) + \left(R_{be} - 2\frac{L_{be}}{\Delta t}\right) \cdot \left((\boldsymbol{K}_b + \boldsymbol{M})^T(\boldsymbol{K}_b + \boldsymbol{M})\right)\right]\Big] \boldsymbol{i}^r_k = 0 \quad (14)$$

in which R_r is resistance of rotor bar, R_{be}, L_{be}, R_{sc}, L_{sc} are resistance and inductance of the end of rotor bar and of the end ring. The elements of the matrix $\boldsymbol{D}_m^r$ is defined

$$D^r_{ij} = -\frac{1}{l^{(m)}}\int_S \beta^r_i \sigma N_j dS \quad (15)$$

in which β^r is one if the integration point belongs to rotor bar, and zero elsewhere, N is shape function in the element method. Eqn. 14 can be written shortly

$$\sum_1^m \boldsymbol{D}^r_m \boldsymbol{A}_{k+1} + \sum_1^m \boldsymbol{D}^r_m \boldsymbol{A}_k + \boldsymbol{C}^r_{k+1}\boldsymbol{i}^r_{k+1} + \boldsymbol{C}^r_k \boldsymbol{i}^r_k = 0 \quad (16)$$

2.2 Equation for stator winding

Because the stator generally consists of fine wires, the current density is assumed to be uniform. The equation for the stator side does not change compared with the FEM model for one slice and can be written

$$\sum_1^m \boldsymbol{K}\boldsymbol{D}^s_m \boldsymbol{A}_{k+1} + \boldsymbol{G}^s \boldsymbol{i}^s_{k+1} + \sum_1^m \boldsymbol{K}\boldsymbol{D}^s_m \boldsymbol{A}_k + \boldsymbol{H}^s \boldsymbol{i}^s_k + \boldsymbol{C}^s(v^s_{k+1} + v^s_k) = 0 \quad (17)$$

in which $\boldsymbol{K}$, $\boldsymbol{G}^s$, $\boldsymbol{H}^s$, and $\boldsymbol{C}^s$ are connection matrices between currents, voltages and vector potentials. The elements of the matrix $\boldsymbol{D}^s$ are defined [9]

$$D^s_{ij} = -\int_{S_n} \frac{l^{(m)} N_{ci}}{S_i} N_j dS_n \quad (18)$$

in which N_{cn} is the number of turns in series in the coil side n. The definition of these matrices and column vector $\boldsymbol{i}^s$ are different for different connections of the stator winding.

2.3 Solution of field and circuit equations

The field equation with current source term is presented in eqn. 5. If all the conductors of an induction machine are taken into account, the two-dimensional field equation becomes

$$\nabla \times (\nu \nabla \times \boldsymbol{A}) + \sigma\frac{\partial \boldsymbol{A}}{\partial t} - \left\{\frac{\sigma}{S_b}\int_S \beta^r_j \frac{\partial \boldsymbol{A}}{\partial t} \cdot dS + \frac{1}{S_b}\sum_{j=1}^{Q_r} \beta^r_j i^r_j + \sum_{j=1}^{p} \beta^s_j i^s_j\right\}\boldsymbol{e}_z = 0 \quad (19)$$

where the β functions are used to define the current regions and S_b is cross-section of the rotor bar. Q_r denotes the number of rotor bars in the solution sector and p is number of phases. Using eqns. 7 and 18, eqn. 19 can be written in a time-stepped form for each slice

$$\boldsymbol{S}(\boldsymbol{A}_{k+1})\boldsymbol{A}_{k+1} + \boldsymbol{B}^r \boldsymbol{i}^r_{k+1} + [\boldsymbol{D}^s]^T \boldsymbol{K}^T \boldsymbol{i}^s_{k+1} + \boldsymbol{S}(\boldsymbol{A}_k)\boldsymbol{A}_k + \boldsymbol{B}^r \boldsymbol{i}^r_k + [\boldsymbol{D}^s]^T \boldsymbol{K}^T \boldsymbol{i}^s_k = 0 \quad (20)$$

Combining eqn. 20 with the circuit eqns. 16 and 17, a system of coupled residual equations $\boldsymbol{f}$ is obtained and it can be written in matrix form

$$\begin{bmatrix} \boldsymbol{f}^1 \\ \cdot \\ \boldsymbol{f}^m \\ \boldsymbol{f}^r \\ \boldsymbol{f}^s \end{bmatrix} = \begin{bmatrix} (\boldsymbol{S}_1) & & & \boldsymbol{B}^r_1 & \boldsymbol{D}^{s\,T}_1 \boldsymbol{K}^T \\ & \cdot & & \cdot & \cdot \\ & & (\boldsymbol{S}_m) & \boldsymbol{B}^r_m & \boldsymbol{D}^{s\,T}_m \boldsymbol{K}^T \\ \boldsymbol{D}^r_1 & \cdot & \boldsymbol{D}^r_m & \boldsymbol{C}^r & \\ \boldsymbol{K}\boldsymbol{D}^r_1 & \cdot & \boldsymbol{K}\boldsymbol{D}^s_m & & \boldsymbol{G}^s \end{bmatrix} \begin{bmatrix} \boldsymbol{A}_1 \\ \cdot \\ \boldsymbol{A}_m \\ \boldsymbol{i}^r \\ \boldsymbol{i}^s \end{bmatrix} + \begin{bmatrix} 0 \\ \cdot \\ 0 \\ 0 \\ h(\boldsymbol{v}^s) \end{bmatrix} = \begin{bmatrix} 0 \\ \cdot \\ 0 \\ 0 \\ 0 \end{bmatrix} \quad (21)$$

3 Results

We have applied our multislice model to the simulation of a three-phase induction motor with cast aluminium rotor and with P = 37kW, f = 50Hz, four poles and skewing of 1.53 stator-slot pitch in the rotor. The motor has 48 stator slots and 40 rotor slots. The same motor has also unskewed rotor for comparison. Taking periodicity conditions for the finite element mesh and circuit equations into account, only one pole has to be modelled. The used finite element has 1510 second-order triangular elements and 3427 nodes. The simulation near the nominal point (1476 rev/min, 400V, 50Hz sinusoidal voltage supply, star connection, Δt = 20ms/400) was done for the model with the numbers of slices m = 1 and m = 3. The rotor skew effects are considered only in the case of m = 3. In Table 1 the calculation results are compared with the measured ones. The values of the slip are taken from the measurements. The measured rotor speed is not exactly the same as the calculated one because the frequency of the supply varies a little bit during the measurements.

Table 1: Comparison between calculated and measured results of multislice model

	Calculated		Measured	
	skewed	unskewed	skewed	unskewed
U, V	400	400	400	400
I_{rms}, A	70.1	68.3	69.4	68.7
P, W	39380	40130	39810	39820
n, rev/min	1473.4	1473.6	1473.9	1472.4
S, %	1.773	1.757	1.773	1.757
T, Nm	242.2	247.3	240	240
P_{out}, W	37370	38160	37040	37110

Fig. 2 shows the flux lines of the first, second and third slice when the total number of slices is three. The rotor skew can be easily seen from the position of the rotor. Figs. 3 and 4 show the measured waveforms of phase voltages and currents of the skewed and unskewed motor. These Figures can be compared with Figs. 5 and 6, in which the calculated waveforms are presented. The effects of skewing are easy to see from Figs. 3–6. The waveforms

are much smoother and the slotting harmonics clearly reduced.

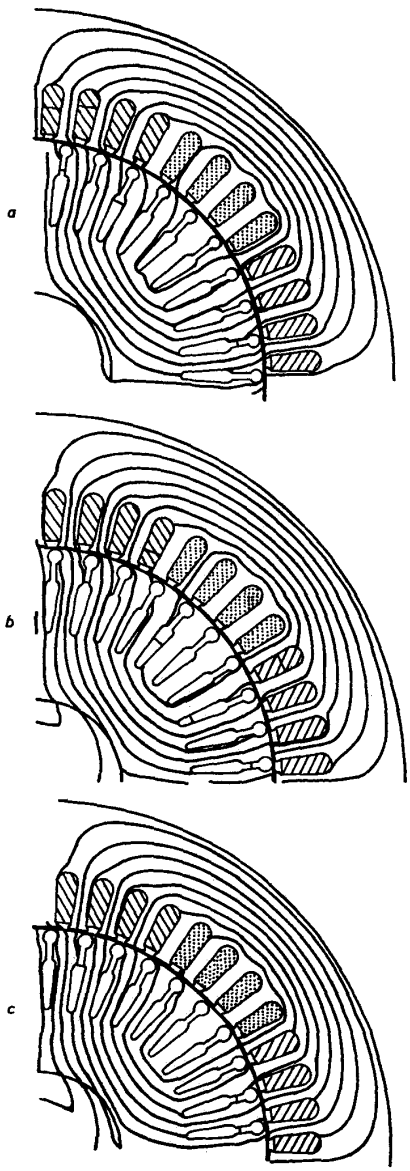

Fig. 2 *Cross-section of machine and flux lines when total number of slices is three*
a First slice
b Second slice
c Third slice

In Table 2 the magnitudes of harmonics of the phase voltages are presented for the skewed and undeskewed case. The magnitudes are calculated by FFT for both, the calculated and measured waveforms. According to Table 2 the use of skewing reduces clearly the amplitude of slot harmonics (19th and 21st).

One of the most familiar effects of rotor skew is the reduction of the torque ripple. Fig. 7 shows the calculated torque for the motor equipped with an unskewed and skewed rotor. The torque is calculated by method based on Maxwell stress tensor [9].

The torque against speed curve (Figs. 8 and 9) is calculated and measured for a skewed and unskewed case. The voltage used was 320V. The calculation was done using three slices and second-order elements.

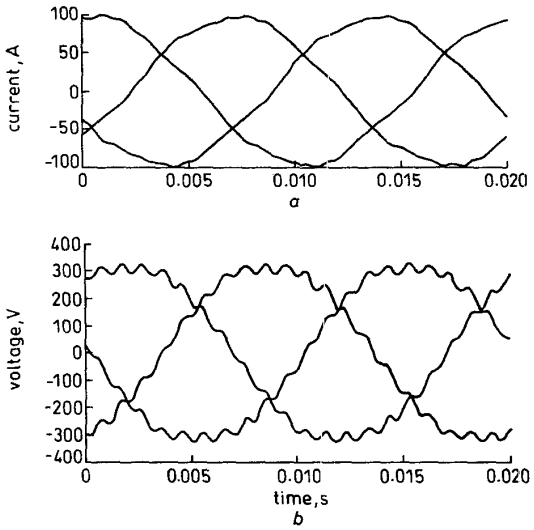

Fig. 3 *Measured voltage and current waveforms for 37kW induction motor with unskewed rotor*
a Current
b Voltage

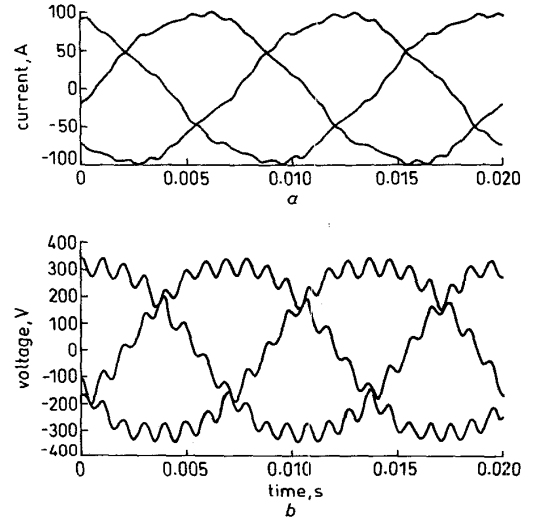

Fig. 4 *Measured voltage and current waveforms for 37kW induction motor with skewed rotor*
a Current
b Voltage

The asynchronous torque dips caused by the fifth harmonic and by the stator-slot harmonics can be clearly seen in the torque curve measured for the unskewed motor. The 19th harmonic causes the large synchronous torque dip at 150 rev/min, and a smaller synchronous torque occurs at −300 rev/min. The skewing reduces the parasitic torques but it does not eliminate completely, for instance, the synchronous torque dips. At the negative speeds the torque measured for the skewed motor increases and becomes even larger than the torque measured for the unskewed machine.

The torque computed for the unskewed motor agrees well with the measured one. For the skewed machine, the agreement is good at the positive speed range but at negative speeds the computed torque is smaller than the measured one. The reason for this behaviour is not quite clear. The division of the machine into three slices is not enough to model properly the higher harmonies with short wavelengths, and this may cause the error in the torque.

An increase of the number of slices from three to five did not change the torque significantly. Maybe more slices are needed to get good results at negative speeds but it increases computation time significantly.

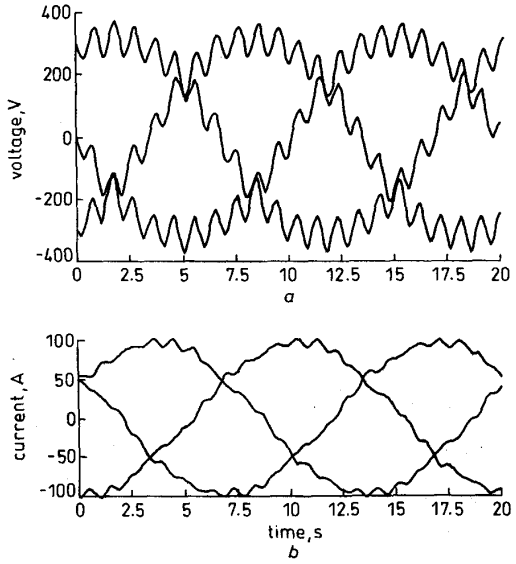

Fig. 5 *Computed voltage and current waveforms for 37kW induction machine modelled using one slice*
a Voltage
b Current

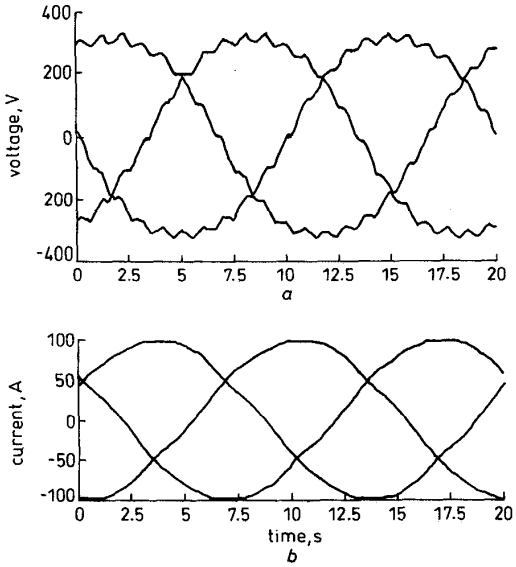

Fig. 6 *Computed voltage and current waveforms for 37kW induction machine modelled using three slices*
a Voltage
b Current

Table 2: Magnitudes of harmonics by FFT from calculated and measured phase voltage waveforms

Order of harmonic	Skewed rotor, V		Unskewed rotor, V	
	measured	calculated	measured	calculated
1	326	326	327	326
3	13.3	13.9	15.3	12.4
19	3.7	2.1	6.9	9.1
21	13.7	11.2	26.9	41.6
22	3.4	2.9	7.5	10.7
23	2.4	1.6	3.6	6.1

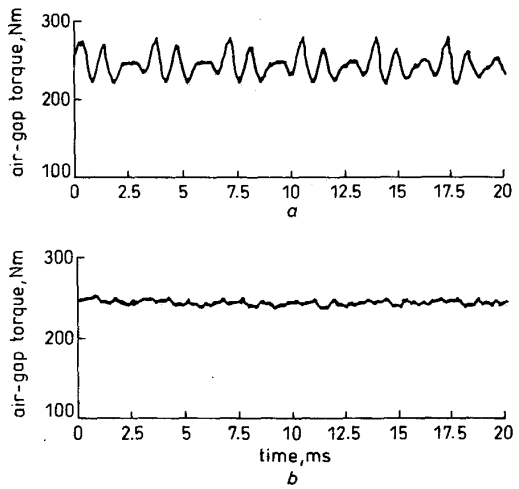

Fig. 7 *Calculated torque as function of time for 37kW induction motor*
a Unskewed rotor
b Skewed rotor

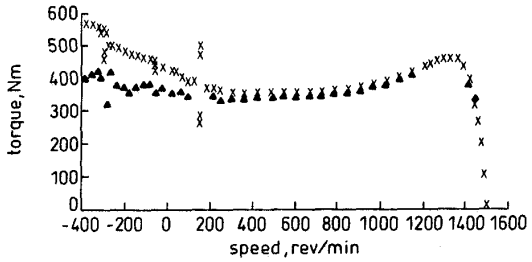

Fig. 8 *Measured and calculated torque against speed curves for 37kW induction motor with skewed rotor slots*
▲ calculated
✳ measured

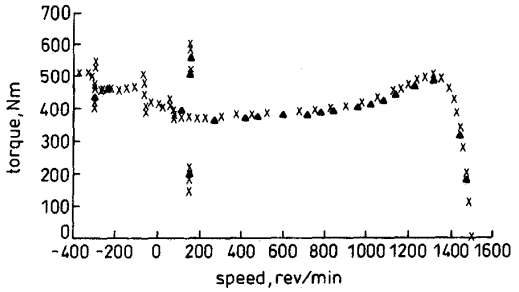

Fig. 9 *Measured and calculated torque against speed curve for 37kW induction machine with unskewed rotor slots*
● measured
✳ calculated

If the difference in the computed and measured torque is associated with underestimation of the harmonic torques, one would expect to see some larger torque dips in the measured curve but it increases relatively smoothly as the speed decreases. Another explanation for the large torque at the negative speed range could be the losses associated with inter-bar currents flowing in the skewed rotor. The slice model neglects these currents.

The CPU time per one period of line frequency is about 207s, 617s and 1039s on a Hewlett-Packard 9000/778 computer for one, three and five slices using first-order elements. The calculation time depends almost linearly on the number of slices. The optimum number of slices is not determined in this work. The bigger the number of slices, the better the results; unfortunately the computation time grows almost linearly with the number of slices.

4 Conclusions

A numerical model permitting the simulation of induction machines with skewed rotor slots has been presented. The two-dimensional finite-element method was used for electromagnetic field analysis of the induction machine. Skew effects are considered by coupling several discs cut by planes perpendicular to the shaft. The slices were connected together by forcing the rotor bar and stator winding currents to be the same in every slice.

As an example of application we have simulated a 37kW induction motor with and without rotor skew at nominal speed. The results obtained from our model are compared with the measured ones. The model gives good results at the normal operating range. It is easy to see the effect of skewing from the waveform of phase voltage and current.

The torque against speed curve is calculated and measured for the same induction machine with and without rotor skew. For the nonskewed case, the computation gave good results at the whole speed range. The torque computed for the skewed motor agrees well at the positive speed range but at negative speeds the computed torque is smaller than measured. The reason for this behaviour is not quite clear. It might be caused by the interbar currents or too small number of the slices used in the computation.

5 References

1 MÜLLER-TOMFELDE, H.: 'The influence of the skew on the magnetic noise, the heating and the oscillating torque'. Doctoral thesis, Institut für elektrishe Maschinen – Technische Hochschule Hannover, Germany, 1962

2 WILLIAMSON, S., FLACK, T., and VOLSCHENK, A.: 'Representation of skew in time-stepped two-dimensional finite-element models of electrical machines', *IEEE Trans.*, 1995, **IA-31**, (5), pp. 1009–1015

3 BINNS, K.J., HINDMARSH, R., and SHORT, B.P.: 'Effect of skewing slots on flux distribution in induction machines', *IEE Proc.-Electr. Power Appl.*, 1971, **118**, (3/4), pp. 543–549

4 NAU, S.: 'Influence of skewed rotor slots on the magnetic noise of three-phase induction motors'. Proceedings of 8th international conference on *Electrical machines and drives*, Cambridge, UK, September 1997, Vol. 444, pp. 396–399

5 GYSELINCK, J., and MELKEBEEK, J.: 'Modelling of electric machines with skewed slots using the two dimensional finite element method: an efficient solving technique', *Sys. Anal. Model. Simul.*, 1995, **18-19**, pp. 559–562

6 HO, S.L., and FU, W.N.: 'A comprehensive approach to the solution of direct-coupled multislice model of skewed rotor induction motors using time-stepping eddy-current finite element method', *IEEE Trans.*, 1997, **MAG-33**, (3), pp. 2265–2273

7 DZIWNIEL, P., and PIRIOU, F.: 'A time-stepped 2D-3D finite element method for induction motors with skewed slots modelling', *IEEE Trans.*, 1999, **MAG-35**, (3), pp. 1262–1265

8 BOUALEM, B., and PIRIOU, F.: 'Modelling of induction motor accounting for skewed slot effects'. Proceedings of international conference on *Electric machines*, Paris, France, 5-8 September 1994, pp. 699–704

9 ARKKIO, A.: 'Analysis of induction motors based on the numerical solution of the magnetic field and circuit equations', *Acta Polytech. Scand Electr. Eng. Ser.*, Helsinki, 1987, (59), pp. 3–97